JOURNAL OF MATERIALS SCIENCE 27 (1992) 6279–6290

In situ straining: crack development in thin foils of Ni_3Al

R. MAURER*
Max-Planck Institut für Metallforschung, Seestraße 92, D-7000 Stuttgart, Germany

Foils of stoichiometric Ni_3Al were deformed *in situ* in a transmission electron microscope. Under plane stress conditions the crack propagated along slip planes, i.e. along {1 1 1} planes. This is in contrast to the intergranular fracture mode of bulk material. In the direction of the crack path, directly in front of the crack tip (but in the plastic zone), inverse dislocation pile-ups developed during straining. These dislocations are screw dislocations with Burgers vectors $\boldsymbol{b} = a\langle 1\,1\,0\rangle$ and $\boldsymbol{b} = a/2\langle 1\,1\,0\rangle$, respectively. Owing to their extremely low Peierls stresses, these dislocations are highly mobile on {1 1 1} planes. Because the slip plane of these screw dislocations is coplanar to the crack plane, the plastic part of the crack development corresponds to shear cracking of the mode III type. Calculation of the local stress intensity factor, k_{Ic}, confirmed that cleavage fracture occurs in mode I deformation, which is typical of the crack characteristics of Ni_3Al foils. Crack behaviour of Ni_3Al is similar to that of simple b c c metals because of the comparable relations of the k values.

1. Introduction

In many investigations an intercrystalline fracture behaviour of the pure Ni_3Al phase has been found [1, 2], even for grain boundaries without segregation [3–9]. Therefore, grain boundaries in this material are considered intrinsically weak. Molecular statics calculations of [1 0 0] twist boundaries indicate, however, that grain boundaries in Ni_3Al should have about the same strength as pure Ni in transcrystalline fracture [10, 11]. Intercrystalline fracture can occur when the ratio of grain-boundary cohesion to yield stress is below 1 [12]. With increasing strain, stresses in pure Ni are diminished by the development of dislocations before the critical fracture stress of the boundary is reached. Owing to the complicated crystal structure, it is more difficult for dislocations in the Ni_3Al phase to develop and move [13, 14]. Therefore, the critical fracture stress of the boundary caused by exterior straining is reached before the material can plastically deform in the grain's interior. As a result the fracture mode changes from transcrystalline to intercrystalline.

However, the fracture behaviour of pure Ni_3Al is only partially explained by the ratio of grain-boundary cohesion to yield stress. Recrystallized Ni_3Al and $Ni_3(AlTi)$ (Ti = 5 at %) without boron show a mixed fracture mode with intercrystalline and transcrystalline components [15]. The transcrystalline fracture surfaces consist of stepped {1 1 1} facets. $Ni_3(Al, Ti)$ (Ti = 10 at %) shows cleavage fracture along {1 0 0} planes. *In situ* straining experiments in the transmission electron microscope revealed that thin foils of undoped Ni_3Al break along {1 1 1} slip band planes [16]. This is contrary to similar experiments by Bond *et al.* [17] who observed that thin foils of the stoichiometric Ni_3Al phase break at grain boundaries.

In situ transmission electron microscopy (TEM) studies were carried out with undoped, stoichiometric Ni_3Al in order to elucidate the mechanism of crack propagation in correlation with dislocations, grain boundaries and stacking faults.

2. Experimental procedure

Ingots of stoichiometrically composed Ni_3Al alloys were produced by vacuum induction melting using Ni and Al of high purity (> 99.9998 wt %). For homogenization, the ingots were heated in an argon atmosphere at 1373 K for 2, 4, 6 and 24 h, respectively, and afterwards quenched in water. After an annealing time of 2 h, investigations of the structure of the specimens showed a homogeneous distribution of aluminium and nickel. Additionally, the composition of the specimens was analysed with a commercial EDS system (Tracor 2000) which was linked with a transmission electron microscope (Jeol 200CX). The lateral resolution was determined by the width of the incident beam which was 20 nm in this experiment. In different regions of each specimen about 15 points were analysed: 5 on the grain boundary and 5 in each adjacent grain, with distances from the grain boundaries of up to ~13 μm. Regions near a crack were also included in the analysis. Grain sizes between 50 and 300 μm were produced by various annealing times.

For investigations by TEM, two different methods of preparation were used in order to avoid effects caused by the preparation.

**Present address*: Baden-Württembergischer Handwerkstag e.V., Heilbronner Strasse 43, Stuttgart, Germany.

0022–2461 © *1992 Chapman & Hall*

(a) Electropolishing: foil specimens (thickness 0.15 mm) were thinned by electropolishing in a double jet apparatus using 9% perchloric acid in methanol at a temperature of 243 K.

(b) Ion-thinning: the foils were carefully polished conventionally and dimple ground to a thickness of 40 μm prior to ion-milling.

Before preparation, the specimens had to be annealed at 1273 K for about 1 h because of the brittleness of the material. They were reannealed after each step of grinding, polishing, or dimpling, in order to reduce the mechanical stress and to avoid cracking during the preparation. In this way, specimens with an electron-transparent area between two holes were obtained. The details of the procedure for specimen preparation for *in situ* straining are described elsewhere [18].

The specimen was mounted between two guide pins and load was applied by retracting the movable pulling rod. By this mechanism an external uniaxial stress of mode I was caused. The relative deformation velocity, v, could be varied from 10^{-8}–10^{-6} m s^{-1}. Owing to the brittleness of Ni_3Al, the velocity used was 10^{-8} m s^{-1}. By applying a load to a TEM specimen only the thinned regions (≤ 30 μm) are considerably deformed. The deformation of the thicker regions (~ 0.5 mm) can be neglected. From Fig. 2a the width of the electron transparent region l is measured as ~ 250 μm. Therefore, the resulting strain rate, ε, was $\varepsilon = v/l = 4 \times 10^{-5}$ s^{-1}. Forces applied to the specimens could not be measured.

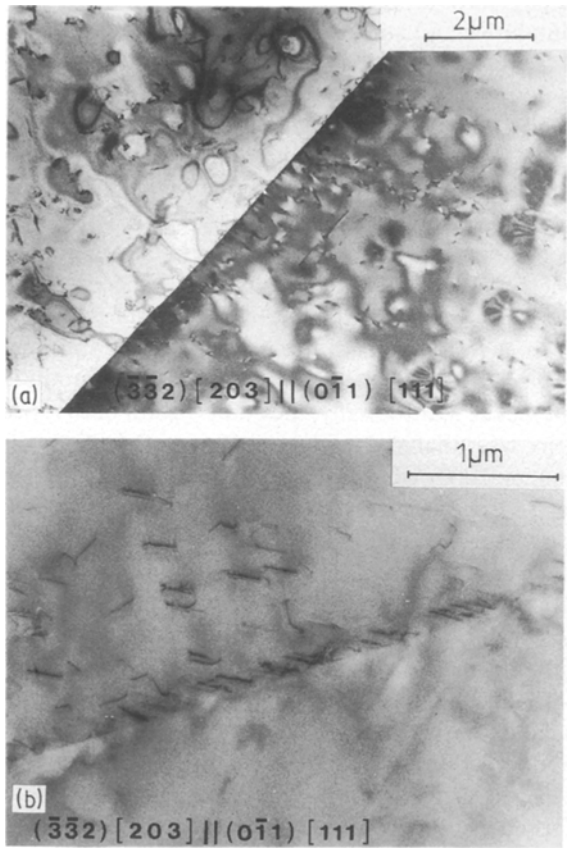

Figure 1 (a) SEM photo of an Ni_3Al specimen with intergranular crack behaviour fractured *in situ* in an AES analyser. (b) Typical AES spectrum measured at a point at the crack surface of (a).

In situ straining experiments were carried out in an AEI EM 7 electron microscope, a 1 MeV high-voltage electron microscope (HVEM). As expected, cracks developed in the thinnest region between the two holes so that the deformation behaviour could be observed in the microscope and recorded on a video tape. The experiments were performed at room temperature under constant displacement conditions. The electron micrographs were taken under stress-applied conditions.

For Auger electron microscopy (AES) analysis, ingots of the same material were annealed at 973 K for 3 h to obtain a high content of segregated atoms at the grain boundaries. Afterwards, the material was spark-cut into samples of a size of 3.6 mm × 32 mm × 16 mm. These samples were notched. AES analysis was carried out with a Perkin–Elmer SAM 595 scanning Auger microprobe. The specimens were fractured *in situ* in the AES equipment (in an ultra-high vacuum at room temperature).

3. Results

3.1. General remarks

Within the accuracy of the EDS analysis, the specimens were homogeneous. The standard deviation calculated from 20 measured values amounts to 0.13 wt %. As expected, no impurities could be detected by EDS in this high-purity material.

Fracture of the Auger samples was of perfect intergranular mode (Fig. 1a), in agreement with observations by Ogura *et al.* [9]. The Auger spectra revealed a minor content of impurities at the grain boundaries (Fig. 2b).

For TEM an electropolished specimen with a large electron transparent area, but without a hole, was obtained. Large regions were free of cracks and bending contours (Fig. 2a). At and within the grain boundary, many regularly distributed dislocations could be observed (Fig. 2b). (The dislocation density was 5×10^8 cm^{-2}). In this specimen area, cracks originated when the specimen was strained. Fig. 3 shows the crack development. This kind of crack is typical of the examined Ni_3Al foils.

When external stress was applied, cracks were initiated at the regions of the highest local stress concentration in the thinnest area between the two holes of the specimen and they propagated in a direction roughly perpendicular to the tensile axis. According to this study, the cracks did not propagate in the grain boundaries, as they do in macroscopic specimens, but in the grain's interior as observed during *in situ* straining of Ni_3Al foils. This behaviour was found to be independent both of the grain size (in a range 50–200 μm) and of the preparation method. Effects like hydrogen loading during specimen preparation might influence the crack propagation mode, but this is improbable because the electric potential of the specimen is positive so that hydrogen loading is unlikely to happen during electropolishing. Additionally, because hydrogen embrittles grain boundaries preferentially [19] it would cause cracks in the boundaries, which is incompatible with observations.

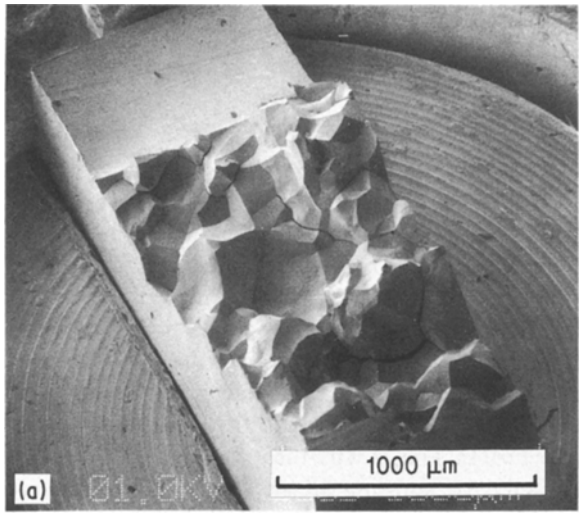

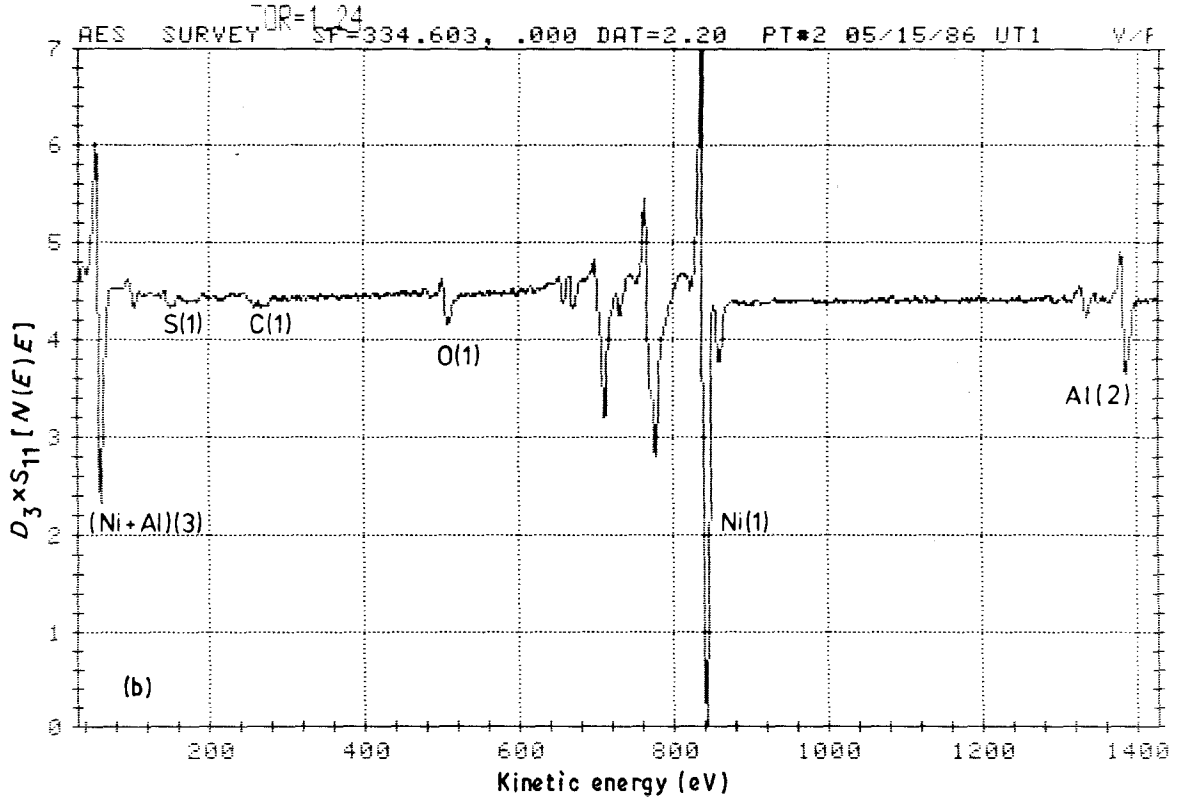

Figure 2 (a) Grain boundary of an electropolished specimen without bending contours or cracks. The orientation relationship of the boundary cannot be described as a special grain-boundary orientation. (b) A higher magnification of the same grain-boundary as in (a) with adequate tilting. In the grain boundary and in the grain's interior many dislocations are present.

3.2. Characterization of the crack

The different phases leading to a crack can be explained by a sequence of micrographs taken during an *in situ* straining experiment. Before deformation only a few dislocations are present (Fig. 4a). When stress is applied, more and more dislocations develop, all of which lie in one plane (Fig. 4b). When the dislocation density in this plane reaches a critical value, a crack originates from the same slip plane (Fig. 4c). Dislocations were emitted from the crack tip during early stages of crack propagation and they spread beyond the crack-tip area. The crack tip continued to send out linear arrays of dislocations having the form of an inverse pile-up coplanar to the crack. The dislocations did not cross-slip out of the original slip plane but remained within a thin ribbon (Fig. 5). The dislocation density was extremely high near the crack tip and decreased very fast with increasing distance from the crack tip. Because the dislocations cannot leave the slip plane, most crack borders showed no dislocations.

For many cracks, the crack propagation is comparable to that in ionic crystals or semiconductors which split along crystallographic cleavage planes. At a crack which was only slightly opened a detailed analysis of the slip geometry showed that the activated slip system is $\{1\,1\,1\}$–$\langle 0\,1\,1\rangle$ which is the only slip system at ambient temperature [20–23]. Also, the crack plane of the Ni_3Al specimens was shown to be $\{1\,1\,1\}$ (Fig. 6a), in agreement with other observations [15, 16]. At a high magnification, it becomes obvious that the crack plane is not atomically flat, but develops only roughly on a $\{1\,1\,1\}$ plane (Fig. 6b). The

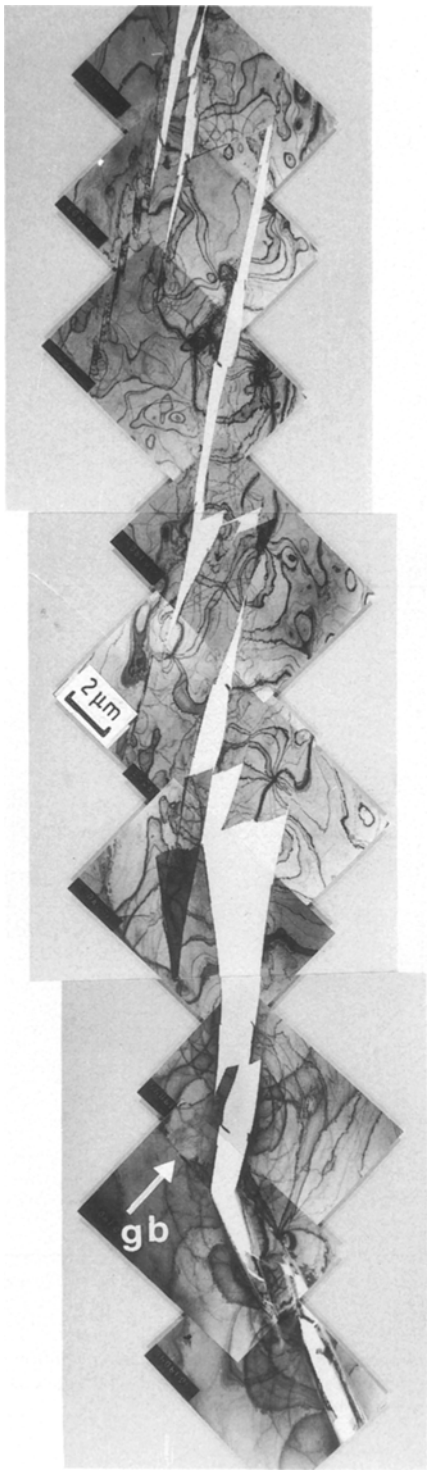

Figure 3 The same specimen as in Fig. 1 after straining. The zig-zag shaped crack propagation is characteristic of the material.

dislocations at the crack tip were found to exist in the pure screw orientation and, as expected [24–26], some were expanded into two super partials connected by a $\{1\,1\,1\}$ antiphase boundary (APB). The Burgers vectors of the screw dislocations which developed during *in situ* deformation were determined as $\boldsymbol{b} = a\langle 1\,1\,0\rangle$, and $b = a/2\ \langle 1\,1\,0\rangle$, respectively. The partial dislocations (of $\boldsymbol{b} = a/2\ \langle 1\,1\,0\rangle$), formed by splitting a complete screw dislocation (of $\boldsymbol{b} = a\langle 1\,1\,0\rangle$), enclose an APB [27]

$$[\bar{1}\,0\,1] = 1/2[\bar{1}\,0\,1] + 1/2[\bar{1}\,0\,1] + \{1\,1\,1\}\,\text{APB} \quad (1)$$

Although the energy of a $\{1\,1\,1\}$ APB, at 111 mJ m^{-2} [28], is relatively high in comparison with other faults like the superlattice intrinsic stacking fault (SISF) with 10 mJ m^{-2}, computer simulations confirmed that the dislocation Reaction 1 is energetically most favourable [29, 30]. In addition, these calculations showed that the dislocation cores of the dissociated $[\bar{1}\,0\,1]$ superpartials are limited to $\{1\,1\,1\}$ planes at low temperatures (up to 200 °C). Therefore, the resistance of the lattice towards of the movement of such dislocation pairs (= Peierls stress) is extremely low. Consequently, these dislocations are extremely mobile on $\{1\,1\,1\}$ planes compared to other partial dislocations (e.g. $a/2\ [2\,\bar{1}\,1]$) or to dislocations on other slip planes (e.g. $\{1\,0\,0\}$). This is why these dislocations with their characteristic splitting are most commonly observed [24–27].

In the vicinity of the crack, many stacking faults and dislocation pile-ups develop in other $\{1\,1\,1\}$ planes, which are parallel to the crack plane (Fig. 7). It may be assumed that on these slip planes the dislocation densities have not yet reached the critical value leading to a crack (Fig. 7b). Many small secondary cracks are observed. They are parallel and seem to form at regular spacings (Fig. 8).

Clearly, the final crack can originate anywhere in the material. A grain boundary is not required for nucleating the crack. Also, the cracks are not initiated at the wedge edge of one of the polished holes (= surface). These smaller cracks develop simultaneously and are initially not connected with each other. With increasing applied stress the original cracks are combined by cross cracks. The resulting zig-zag line is characteristic of this material and was also observed for specimens doped with boron (0.1 wt % B) (Fig. 9). In addition, a step-like crack development can result from the activation of a secondary slip system [31], which may be caused by an external tension axis different from the $\langle 1\,1\,0\rangle$ direction of the primary slip system. For Ni_3Al at room temperature, secondary slip systems are of the type $\{1\,1\,1\}\ \langle 0\,1\,1\rangle$ [24].

3.3. Interaction with grain boundaries

When the crack passes a grain boundary, it changes its direction so as to follow the $\{1\,1\,1\}$ plane in the next grain. However, depending on the orientation relationship of the grains and on the position of the boundary plane, several different situations are possible.

1. The crack crosses the grain boundary (Fig. 10). The position of the $\{1\,1\,1\}$ plane of the adjacent grain favours propagation of the crack into that grain.
2. The crack is reflected at the grain boundary (Fig. 11). $\{1\,1\,1\}$ planes of the second grain are more adverse to the crack than another $\{1\,1\,1\}$ plane of the first grain. This $\{1\,1\,1\}$ plane forms an angle of $\sim 70°$ with the $\{1\,1\,1\}$ crack plane.
3. The crack switches to a different $\{1\,1\,1\}$ plane before reaching the boundary (Fig. 12). The region between grain boundary and crack is highly deformed.
4. When the crack reaches a boundary, which itself is a $\{1\,1\,1\}$ plane, the crack follows that boundary

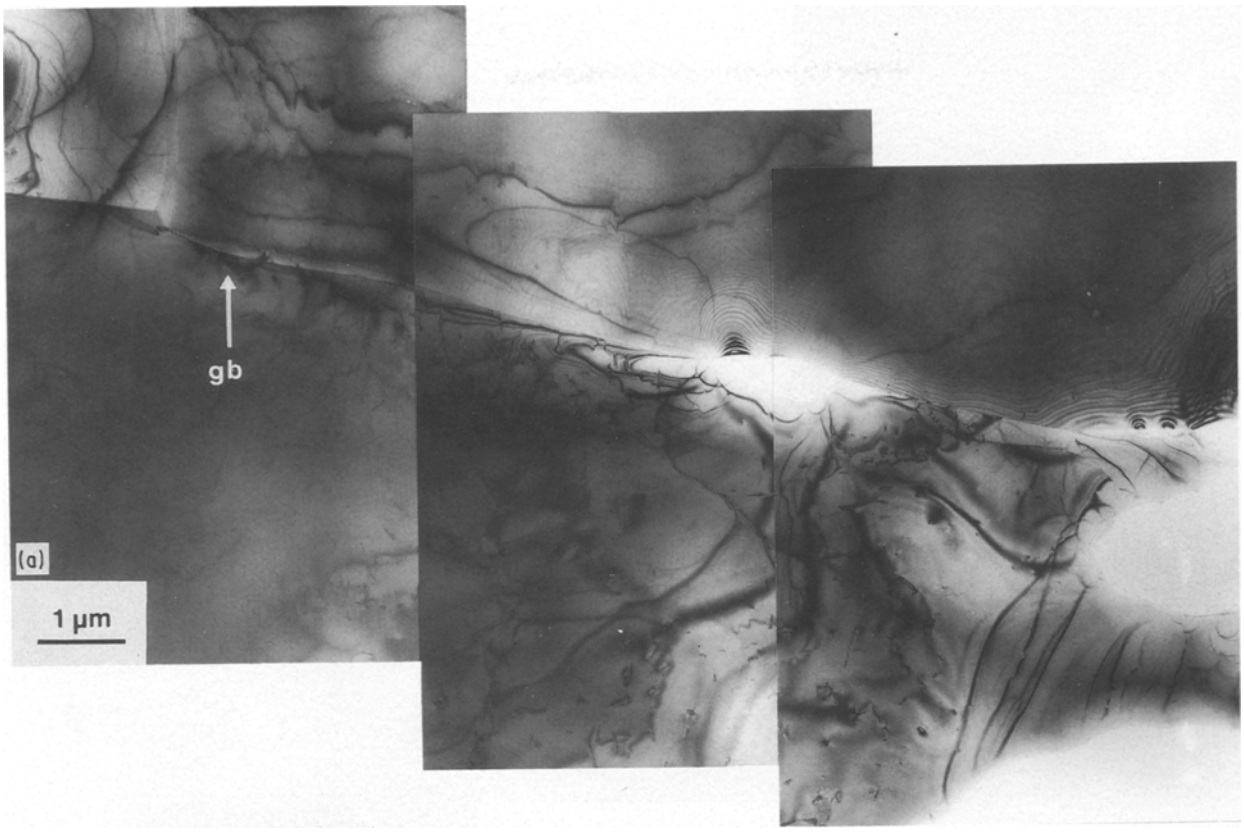

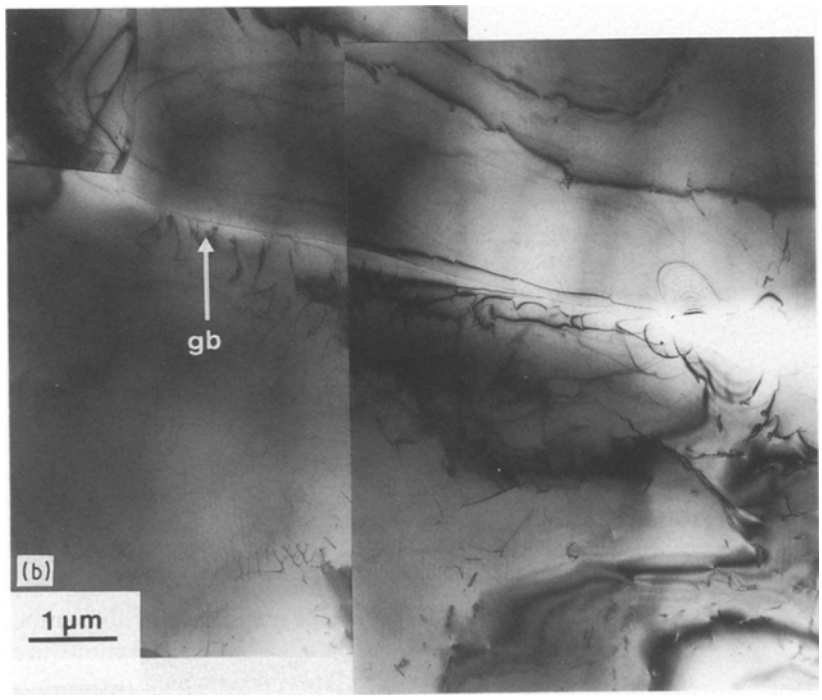

Figure 4 (a) An ion-thinned specimen before deformation: few dislocations are present. (b) The same specimen as in (a) during straining: dislocations develop on slip planes (= {1 1 1} planes). (c) A crack that forms during further deformation in the slip plane.

until it deviates again under the influence of the local stress system (Fig. 11).

5. A crack runs parallel to a boundary which lies in a {1 1 1} plane (Fig. 13). Both the grain boundary and the (1 1 1) plane in the interior of the grains are favourable crack paths; the latter path is preferred and the material does not fracture at the boundary.

6. Despite variation in specimen preparation and annealing time no cracks were observed to propagate exclusively on grain boundaries. Aside from the special case (Fig. 11) of a grain boundary coinciding with a {1 1 1} plane, the cracks in all investigated specimens propagated in a purely transcrystalline manner. All in all, about 40 grain boundaries were examined. These observations prove that the grain boundaries in thin Ni_3Al foils are not intrinsically weak. These results can hardly be due to the special conditions in the foils: during specimen preparation the boundaries were corroded more than their vicinity. This notch effect should make grain boundaries in such thin foils even more fragile than those in the bulk material.

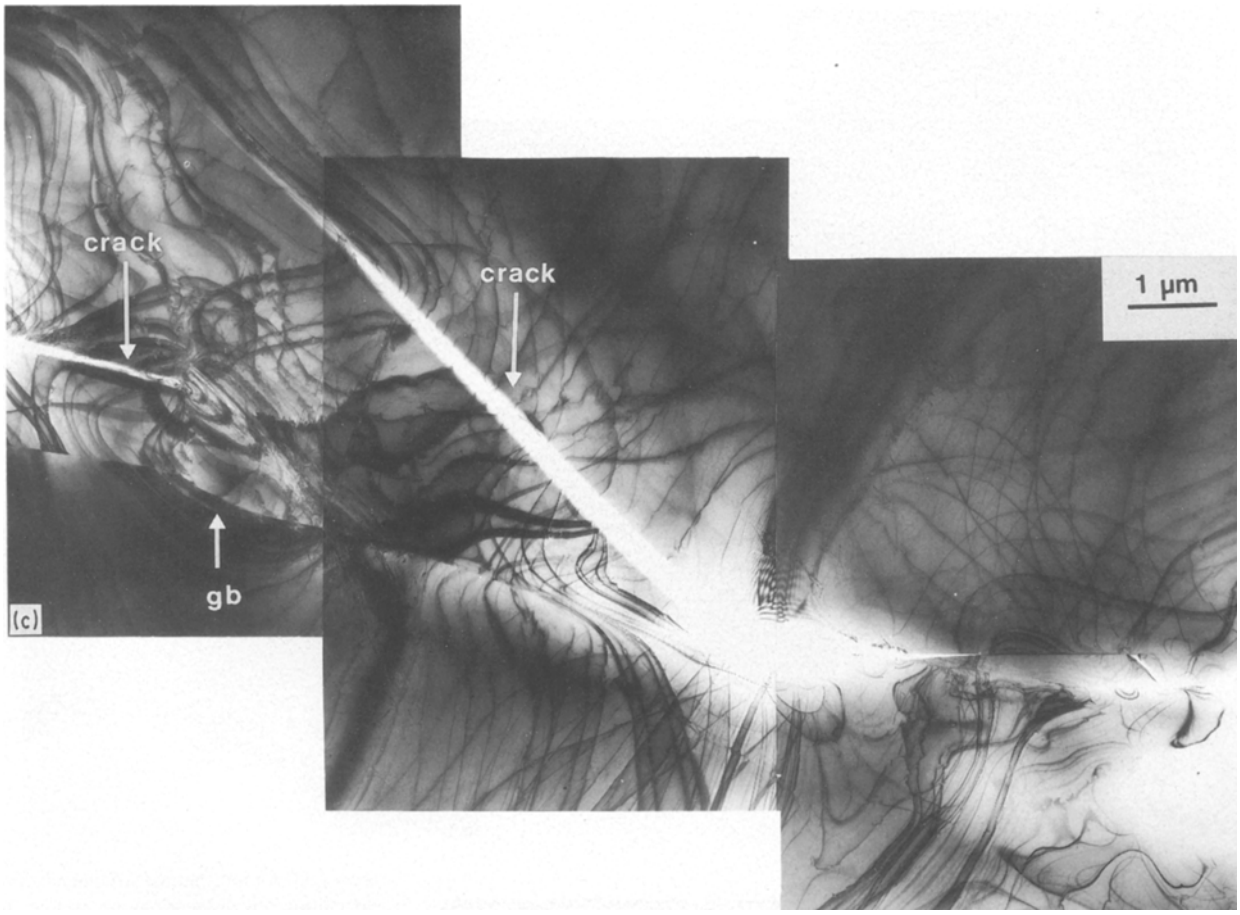

Figure 4 Continued.

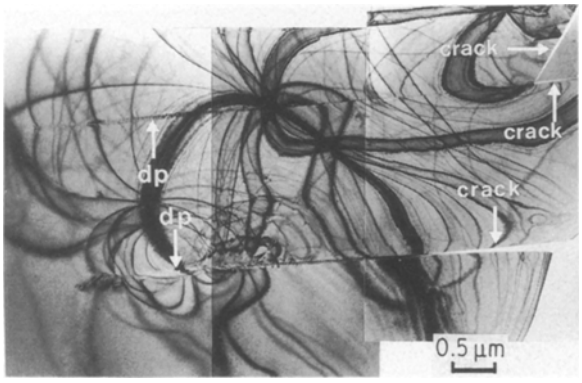

Figure 5 A crack not yet opened where inverse dislocation pile-ups are sent out from the crack tips. The crack borders are nearly without dislocations (same specimen as Fig. 1).

4. Discussion

Recently, the distribution of dislocations in the plastic zone ahead of a crack tip has been studied for various metals during *in situ* tensile deformation in an electron microscope [31]. The crack tip geometry in a foil specimen of Ni_3Al is similar to that observed in stainless steel [32], copper [33] and, to a large extent, nickel [34]. In all these cases the plastic zone was coplanar with the crack plane; the dislocations in the plastic zone had the form of an inverse pile-up lying in a thin ribbon, and the cracks were identified as anti-plane strain shear cracks of screw dislocations of the mode III type. This common feature reflects the low stacking fault energy of these metals in comparison with the line energy of the corresponding dislocations: in metals with a high stacking fault energy the dislocations cross-slipped out of the original slip plane and formed a broad plastic zone [31].

According to Ohr [31], the deformation behaviour at the crack tip is determined by the loading mode (see Fig. 14). To discuss the criteria for ductile versus brittle behaviour for the three different loading modes, the local critical stress intensity factors of both fracture types must be calculated and compared.

Concerning the ductile deformation, mode I generates edge dislocations on slip planes inclined towards the crack plane. Mode II is characterized by edge dislocations on slip planes coplanar to the crack plane. In mode III, coplanar screw dislocations are developed. Unlike thick specimens which prefer modes I and II, a thin foil is free to deform in mode III, as indicated by the present observations. Because of the screw character of the dislocations generated at the crack tip, the plastic zone in thin foils represents a pure shear deformation of the mode III type.

The critical local stress intensity factors, k_e, for dislocation generation and emission are given by Ohr [31] for the different modes

$$k_{Ie} = \frac{2}{\sin\phi_1 \cos 1/2\,\phi_1}\left[\frac{\mu b}{(1-\nu)(8\pi r_c)^{1/2}} + (2\pi r_c)^{1/2}\left(\sigma_f + \frac{B\sin\phi_1}{r_c^2+\beta^2}\right)\right] \quad (2)$$

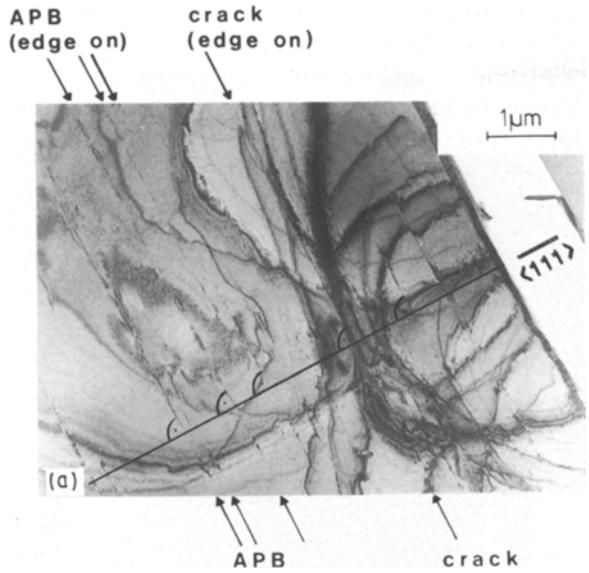

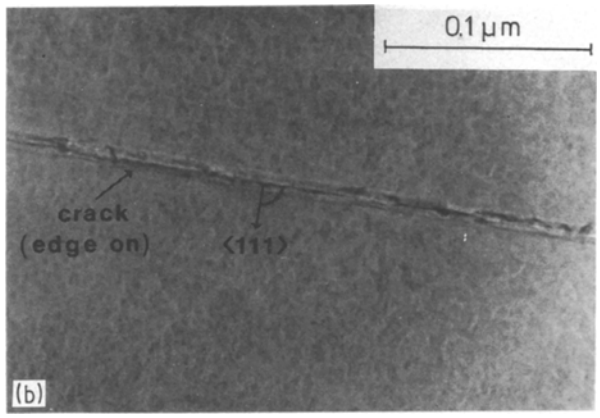

Figure 6 (a) General view of a crack only slightly opened, with the plane being normal to the electron beam (edge-on position). (b) Magnification of (a) showing the microstructure of the crack plane (same specimen as Figs 1 and 3).

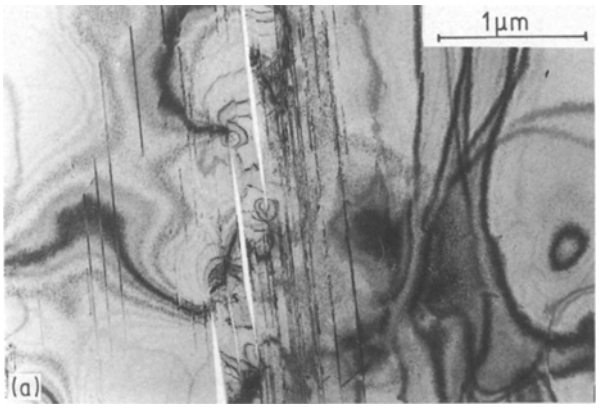

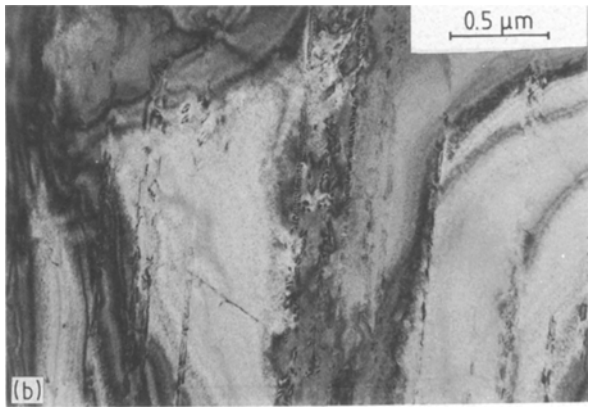

Figure 7 (a) Slightly opened cracks with parallel stacking faults in the {1 1 1} planes. (b) High dislocation densities coplanar to already emerged cracks not situated in the immediate crack region.

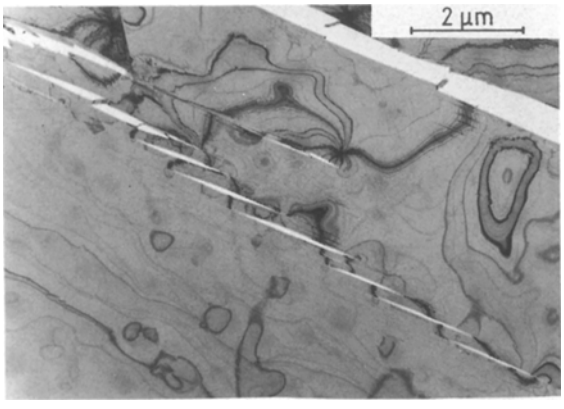

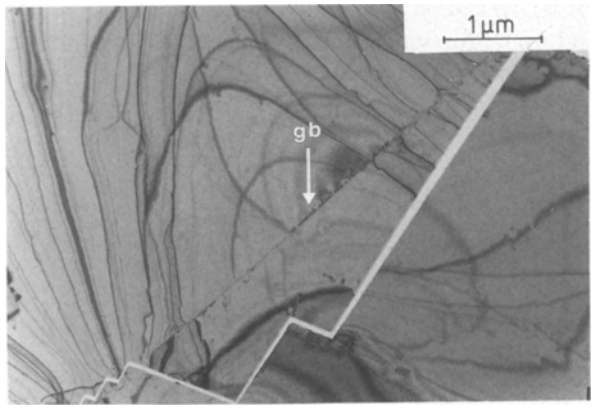

Figure 8 Small, parallel cracks with a characteristic length of 1.23 (± 0.64) μm and a defined distance of 0.11 (± 0.07) μm.

Figure 9 Typical zig-zag crack characteristic of this material (in this special case: specimen doped with boron).

$$k_{\mathrm{IIe}} = \frac{\mu \boldsymbol{b}}{(1-\nu)(8\pi r_c)^{1/2}} + (2\pi r_c)^{1/2}\,\sigma_f \qquad (3)$$

$$k_{\mathrm{IIIe}} = (2\pi r_c)^{1/2} \sec 1/2\,\phi_3 \left(\frac{\mu \boldsymbol{b}}{4\pi r_c} + \sigma_f\right) \qquad (4)$$

where $B = 2\gamma\beta$, $\beta = r_c e^{3/2}$, γ is the effective fracture surface energy, r_c the inner cut-off radius of the dislocations, σ_f the friction stress ($\approx$ yield stress), ν Poisson's ratio and μ the shear modulus. ϕ is the angle between slip and crack plane calculated for minimum k_{Ie} and k_{IIIe} values (for k_{Ie} $\phi_1 \approx 70°$, for k_{IIIe} $\phi_3 = 0°$). The values of γ, μ, σ_f, etc., are taken from previous studies [35–41] (Table I). As Fig. 15a shows, the k_e values crucially depend on the value of $r_c/\boldsymbol{b}$. Using a non-linear Peierls–Nabarro model for fcc materials

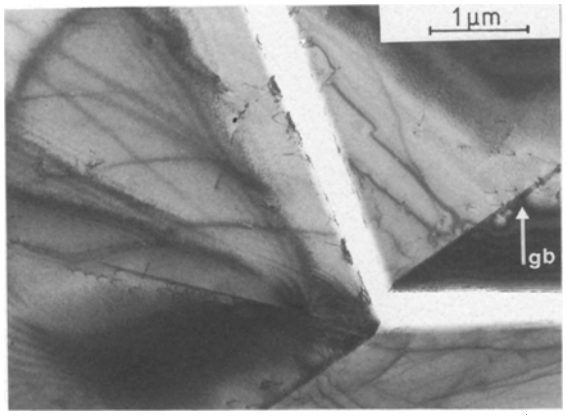

Figure 10 Crack propagating in a {1 1 1} plane before and after passing the grain boundary. This is in contradiction to macroscopical investigations.

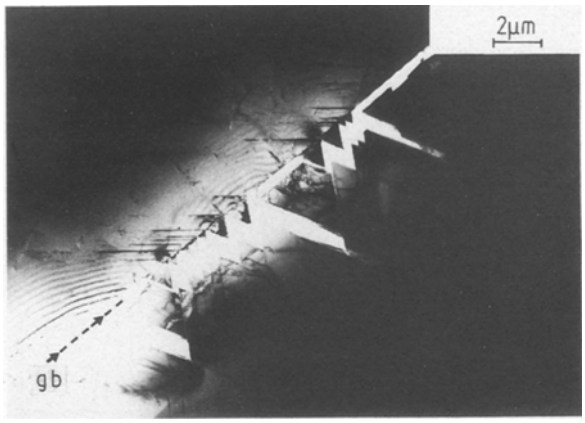

Figure 11 A crack reflected at a grain boundary. (Part of it runs into the grain boundary, then turns aside.)

[42], the value of $\boldsymbol{b}\, c_{44}/\gamma_{SF}$ determines $r_c/\boldsymbol{b}$, where c_{44} is the elastic shear modulus and γ_{SF} the stacking fault energy. On the basis of the data listed in Table I, $r_c/\boldsymbol{b}$ for Ni_3Al can be estimated as 2.1 for edge dislocations and as 1.3 for screw dislocations in comparison with 0.89 (edge) and 0.55 (screw) for Ni. As Fig. 15a shows, the following relation is valid independent of r_c

$$k_{Ie} > k_{IIe} > k_{IIIe} \tag{5}$$

Therefore, if the applied stress intensities, K, were equal for all three modes of deformation, local mode III deformation (involving the emission of coplanar screw dislocations from the crack tip) would be favoured in agreement with the experimental results.

The condition for brittle fracture can be expressed in terms of the local critical stress intensity factor, k_C, [43, 44]. Thus, we have

$$k_{Ic} = k_{IIc} = [4(1 + \nu)\mu\gamma]^{1/2} \tag{6}$$

$$k_{IIIc} = (4\mu\gamma)^{1/2} \tag{7}$$

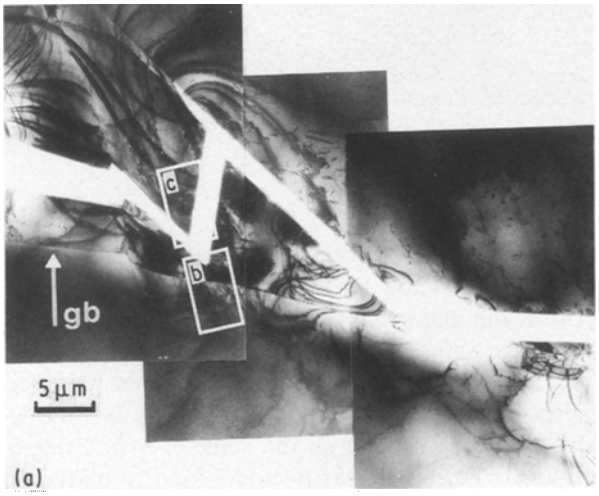

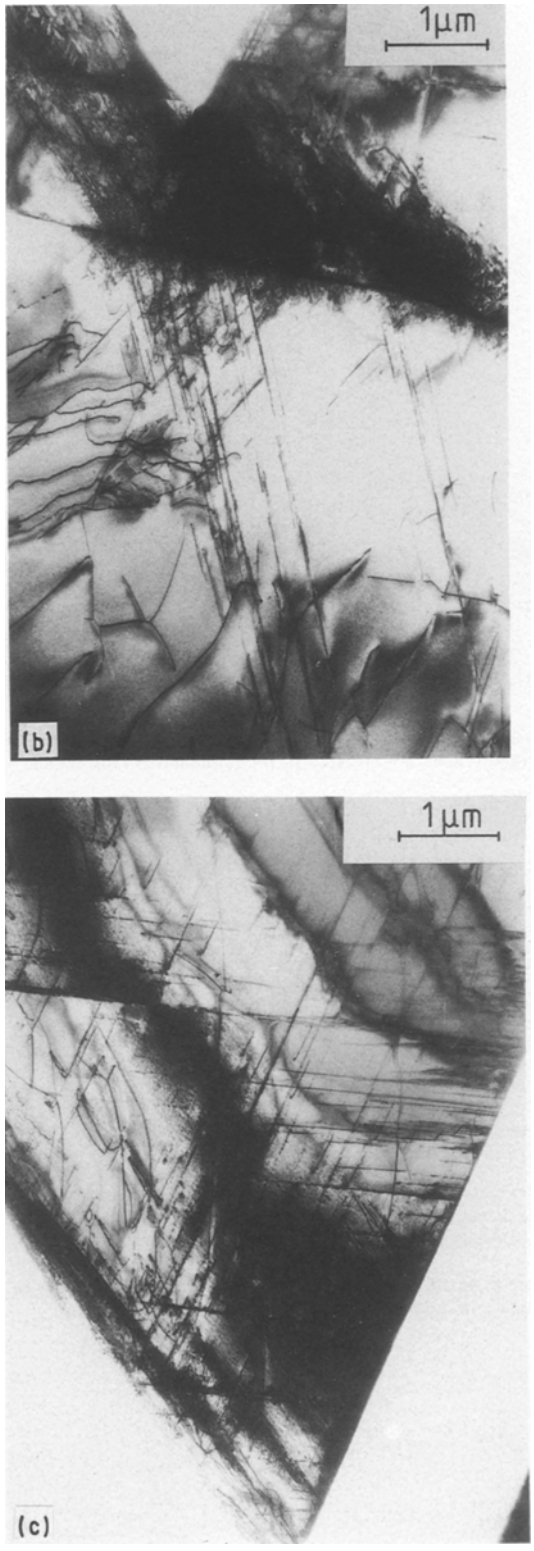

Figure 12 (a) A crack that changes its direction before reaching the grain boundary (overview). (b) The region between grain boundary and crack is strongly deformed. (c) The opposite "corner".

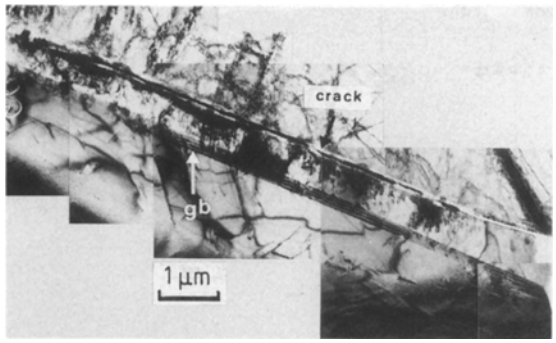

Figure 13 Crack parallel to a grain boundary.

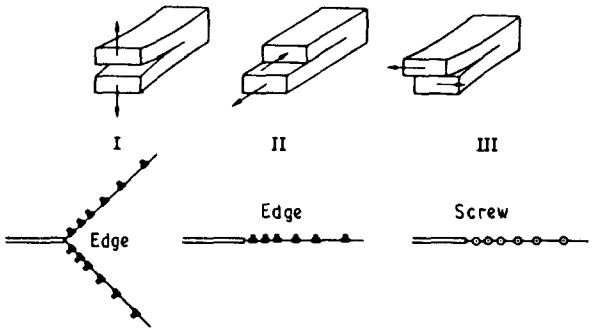

Figure 14 Three modes of fracture and crack tip deformation. I, opening mode; II, sliding mode; III, tearing mode (from [29]).

for plane stress (thin foil), and

$$k_{Ic} = k_{IIc} = \left(\frac{4\mu\gamma}{1-\nu}\right)^{1/2} \quad (8)$$

$$k_{IIIc} = (4\mu\gamma)^{1/2} \quad (9)$$

for plane strain (bulk material).

Table I shows the room-temperature values, k_c, calculated for Ni_3Al. Owing to the similarity of the elastic constants, the values for Ni_3Al are of the same magnitude as those for Ni. Fig. 15b shows the ratios of k_e/k_c for Ni_3Al as a function of the assumed r_c values. In the loading conditions of mode II or III, the value of k_e is smaller than that of k_c for all values of r_c. This means that crack tip deformation is always favoured in comparison with brittle fracture as far as modes II and III are concerned. In mode I, two possibilities exist

1. for $r_c < 2.6\boldsymbol{b}$: $k_{Ie} > k_{Ic}$ (brittle) (10a)
2. for $r_c > 2.6\boldsymbol{b}$: $k_{Ie} < k_{Ic}$ (ductile) (10b)

If $r_c < 2.6\boldsymbol{b}$ is correct, the brittle fracture behaviour of mode I in Ni_3Al can be explained in analogy to the semibrittle nature of some b c c metals, like Fe, W, Mo, etc. (For $k_e \approx k_c$, crack tip deformation and brittle crack growth are expected to occur simultaneously.) These semibrittle b c c metals fail by cleavage after a small amount of crack tip deformation.

Cracks often propagate as a result of cleavage in mode I while crack tip deformation occurs either in mode II or in mode III. The crack tip can only be blunted by the emission of edge dislocations into planes inclined to the crack plane. However, this behaviour does not apply to Ni_3Al because the relation $k_e < k_c$ is valid for coplanar dislocation emission. In electron microscope studies of crack tip deformation in several f c c and b c c materials, Ohr [31] frequently observed a combined loading of mode I and mode III for cracks along crystal slip planes. The same effect appears in Ni_3Al foils. As the straining experiments reveal, screw dislocations coplanar to the future crack were produced in the plastic zone of Ni_3Al, indicating a deformation in pure mode III. The vanishing relative displacement of the crack flanks proves the presence of an additional component of mode I. The zig-zag shaped crack path, as shown in Fig. 9, can only appear if mode I cleavage fracture is accompanied by a deformation of the crack tip in mode II as is also shown in Fig. 9. Based on the calculated k values for Ni_3Al (k_e and k_c for all three modes, see Tables I and II), the results of the experiments can be interpreted as follows

$$k_{IIe} < k_{IIc} = k_{Ic} \quad (11a)$$

$$k_{IIIe} < k_{IIIc} < k_{Ic} \quad (11b)$$

$$k_{IIIe} < k_{IIe} \quad (11c)$$

These relations lead to plastic deformation in Ni_3Al preferentially in mode III (and to a smaller extent in mode II). With increasing external load the local stress intensity k_{III} increases until it reaches the critical value k_{IIIe}. When k_{III} is further increased to energize the emission of dislocations, the local stress remains at the value k_{IIIe}. Additional dislocations are emitted under

TABLE I Comparison of some parameters of Ni_3Al and pure Ni

Parameter		Ni_3Al	Ni
{1 1 1} surface energy, γ (mJ m^{-2})		1645 [36]	1725 [39]
Shear modulus, μ (10^{11} N m^{-2})		0.78 [37]	0.85 [37]
Poisson's ratio, ν		0.299 [37]	0.300 [37]
Lattice friction stress ($\approx$ yield stress) (MPA)		138 [38]	34 [40]
Burgers vector, $\boldsymbol{b}$ (nm)		5.04 (Present work)	2.49 [41]
Critical stress intensity factors for brittle fracture (10^5 N m$^{-3/2}$)			
$k_{Ic} = k_{IIc}$	plane strain	8.6 (Present work)	8.8 [29]
$k_{Ic} = k_{IIc}$	plane stress	8.2 (Present work)	8.3 [29]
k_{IIIc}	plane strain/plane stress	7.2 (Present work)	7.2 [29]
Stacking fault energy (mJ m^{-2})		111 $\pm$ 15 [26]	125 [42]
Elastic constants	c_{44}	1.25 [37]	1.22 [37]
	c_{12}	1.44 [37]	1.50 [37]
	c_{11}	2.19 [37]	2.47 [37]

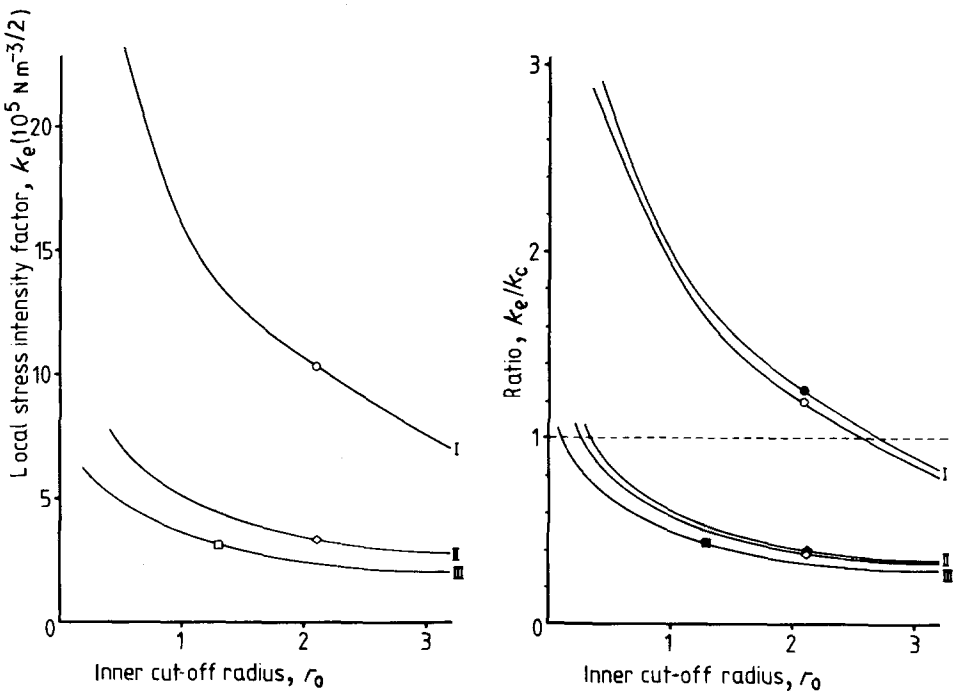

Figure 15 (a) Critical stress intensity factors, k_c, for dislocation generation as a function of the r_c value ($\boldsymbol{b}$ = value of the Burgers vector of the a_0 ⟨1 1 0⟩ superdislocation). (○) k_I, (◇) k_{II}, (□) k_{III}. (b) ratio k_e/k_c as a function of the r_c value for the different deformation modes: (○, ●) Mode I, (◇, ◆) mode II, (□, ■) mode III, for (○, ◇, □) plane strain and (●, ◆, ■) plane stress.

the influence of the external stress so that the local stress intensity hardly exceeds the k_{IIIe} value. The external load determines the number of dislocations created. A similar mechanism is valid for edge dislocations generated in mode II deformation. However, the k_{IIe} value for Ni_3Al is relatively high so that few edge dislocations will be generated. The screw dislocations under mode III (and the edge dislocation in mode II) do not influence the k_I value. Whereas the local k_{III} value (and the k_{II} value, respectively) remains constant with increasing applied load, the local k_I value continues to rise until it reaches the critical value k_{Ic} and cleavage fracture mode I leads to material failure. Consistent with the arguments of Yoo and King [45], cleavage in the case of the mixed mode I and III is most likely to occur on the {1 1 1} plane rather than the other two possible cleavage planes {0 0 1} and {0 1 1}. In a further study [46], they analysed the role of interaction between slip dislocations and symmetric CSL-[1 1 0] tilt boundaries in crack nucleation for the fcc and $L1_2$ structures. For Ni_3Al, no intergranular fracture can be predicted for these grain-boundary types. Only the case that a symmetric double pile-up of primary slip dislocations from both sides of the boundary occurs simultaneously is an exception. This formation is, however, an event of very low probability.

Using the embedded atom method (EAM), atomistic simulations have calculated for Ni_3Al that the effective fracture surface energy has nearly the free-energy value throughout the crack initiation process [35]. Therefore, a nucleated crack will extend automatically [47].

5. Comparison with NiAl foils

The brittle fracture behaviour along cleavage planes observed for Ni_3Al foils is absolutely different from that of NiAl foils. During the deformation of NiAl at a low temperature (up to 600 °C) only perfect screw dislocations of the type ⟨1 0 0⟩ develop [48]. These dislocations do not split into partials because of the high APB energy (~ 400 mJ m^{-2}) [49]. In contrast to Ni_3Al, this fact allows dislocation climb which has, in fact, been observed. Therefore, the crack borders are not dislocation-free (Fig. 16b) and the crack path is not limited to special crystallographic planes (Fig. 16a). The high brittleness of polycrystalline NiAl at temperatures up to 600 °C is caused by an insufficient number of slip systems (Mises criterion). Instead of the necessary five slip systems, only three are present: {1 1 0} ⟨1 0 0⟩ and {1 0 0} ⟨1 0 0⟩ [48]. Also, the activation of cross-slip systems of the ⟨1 0 0⟩ zone does not provide truly independent slip systems [48]. Possible additional deformation mechanisms like twin formation are suppressed as a result of the B2 order [50].

6. Conclusions

In the present study of thin foils, only cracks along {1 1 1} slip planes were observed. This seems to be in contradiction to several investigations concerning completely intercrystalline fracture behaviour of γ′-phase which have been invoked as evidence of the so-called intrinsic weakness of grain boundaries [1–9]. Besides purity and stoichiometric deviations, other parameters such as annealing time and temperature, grain size and loading conditions also determine the fracture path.

The external uniaxial stress in mode I leads to a local deformation of mode I resulting in brittle fracture. The most likely brittle fracture path is cleavage along {1 1 1} in comparison to other planes and to grain boundaries. In general, the tensile axis does not

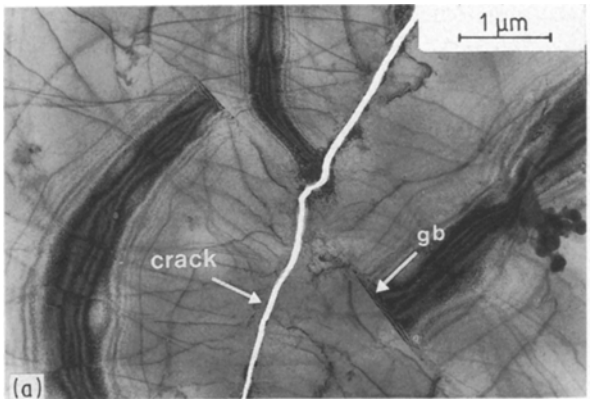

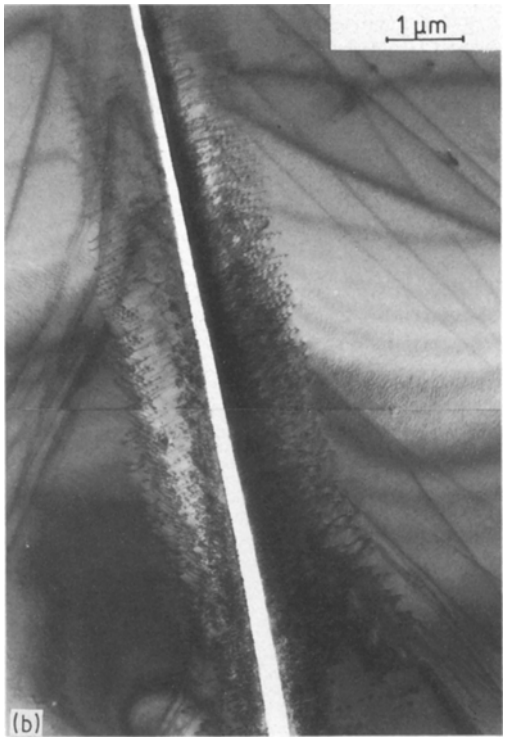

Figure 16 (a) Crack propagation in NiAl; caused by missing slip systems, the crack development is not fixed to a defined plane. (b) A band of dislocations found at the crack borders of NiAl with a width characteristic of this material.

lie exactly in a ⟨1 1 1⟩ crystal direction, normal to the cleavage plane. Therefore, the material deforms by other loading modes in which plastic deformation occurs. A thin foil is free to deform in mode III, developing easily mobile screw dislocations. Deformation in mode II is typical for bulk material, involving the generation of edge dislocations nearly immovable in Ni_3Al. The different dislocation features connected with the change of the local loading condition is considered the reason for the difference in the fracture path. Indeed, with increasing specimen thickness, the fracture path changes from the transcrystalline to the intercrystalline type. The TEM specimen shown in Fig. 17 confirms this statement: the thin specimen region (near the hole) shows the typical zig-zag shaped cleavage fracture. On the other hand, in the thicker region (towards the edge), the specimen has fractured along the grain boundaries.

The different loading conditions may also be the reason why statements like "cleavage fracture in thin foils, grain-boundary fracture in the bulk material"

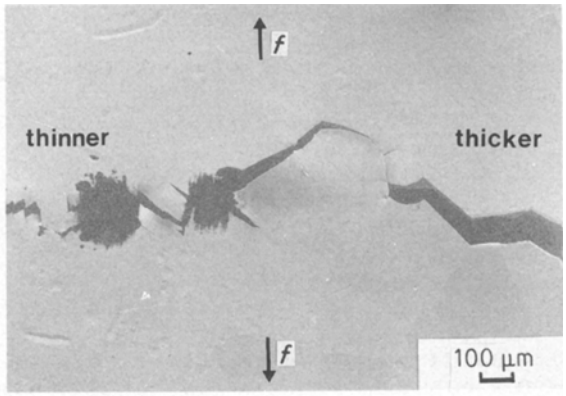

Figure 17 Scanning electron micrograph of a TEM specimen after straining: the crack path changes from intercrystalline to transcrystalline.

are not always correct concerning the γ′-phase. Bond *et al.* [17], for example, found grain-boundary fracture in thin foils, Hanada *et al.* [15] observed cleavage fracture in the bulk material. A transcrystalline crack in the pure γ′-phase, however, always develops along {1 1 1} slip planes.

Acknowledgement

The author thanks the DFG (Deutsche Forschungsgemeinschaft) for financial support.

References

1. O. IZUMI, *Trans. JIM* **19** (1978) 203.
2. C. L. WHITE and D. F. STEIN, *Metall. Trans.* **9A** (1978) 13.
3. K. AOKI and O. IZUMI, *Nippon Kinzoku Gakkaishi* **43** (1979) 1190.
4. C. C. KOCH, J. A. HORTON, C. T. LIU, O. B. CAVIN and J. O. SCARBOROUGH, in "Proceedings of the 3rd International Conference on Rapid Solidification", edited by R. Mehrabian (NBS Gaithersburg, Maryland, 1982) pp. 264–9.
5. C. T. LIU, C. L. WHITE, C. C. KOCH and E. H. LEE, in "Proceedings of the Symposium on High Temperature Materials Chemistry II", edited by Z. S. Munir and D. Cubricciotti (The Electrochemical Society, 1983) pp. 32–41.
6. E. M. SCHULSON, D. L. DAVIDSON and D. VIENS, *Metall. Trans.* **14A** (1983) 1523.
7. A. I. TAUB, S. C. HUANG and K. M. CHANG, *ibid.* **15A** (1984) 399.
8. C. T. LIU, C. L. WHITE and J. A. HORTON, *Acta Metall.* **33** (1985) 213.
9. T. OGURA, S. HANADA, T. MAZUMOTO and O. IZUMI, *Metall. Trans.* **16A** (1985) 441.
10. S. P. CHEN, A. F. VOTER and D. J. SROLOVITZ, *Scripta Metall.* **20** (1986) 1389.
11. S. M. FOILES, in "High Temperature Ordered Intermetallic Alloys II", edited by N. S. Stoloff, C. C. Koch, C. T. Liu and O. Izumi, Materials Research Society Proceedings, Vol. 81 (MRS, Pittsburg, PA, 1987) p. 51.
12. J. E. HACK, D. J. SROLOVITZ and S. P. CHEN, *Scripta Metall.* **20** (1986) 1699.
13. C. T. LIU and J. O. STIEGLER, *Science* **22** (1984) 636.
14. N. S. STOLOFF and R. G. DAVIS, "The Mechanical Properties of Ordered Alloys", in "Progress in Materials Science", Vol. 13, edited by B. Colmers and W. Hume-Rothery (1966).
15. S. HANADA, M. S. KIM, S. WATANABE and O. IZUMI, *Scripta Metall.* **21** (1987) 277.
16. I. BAKER, E. M. SCHULSON and J. A. HORTON, *Acta Metall.* **35** (1987) 1533.
17. G. M. BOND, I. M. ROBERTSON and H. K. BIRNBAUM, *J. Mater. Res.* **2** (1987) 436.
18. R. MAURER and U. SALZBERGER, *Metallography*, in press.

19. A. K. KURUVILLA and N. S. STOLOFF, *Scripta Metall.* **19** (1985) 84.
20. B. H. KEAR and M. F. HORNBECHER, *Trans. ASM* **59** (1966) 155.
21. P. H. THORNTON, R. G. DAVIES and T. L. JOHSTON, *Metall. Trans.* **1** (1970) 207.
22. S. TAKUCHI and E. KURAMOTO, *Acta Metall.* **21** (1973) 415.
23. A. E. STATON-BEVAN and R. D. RAWLINGS, *Phys. Status Solidi (a)* **29** (1975) 613.
24. *Idem., Phil. Mag.* **32** (1975) 787.
25. I. BAKER and E. M. SCHULSON, *Phys. Status Solidi (a)* **89** (1985) 163.
26. A. BALDAN, *ibid.* **75** (1983) 411.
27. D. P. POPE and S. S. EZZ, *Int. Metals Rev.* **29** (1984) 136.
28. J. DOUIN, P. VEYSSIÈRE and P. BEAUCHAMP, *Phil. Mag. A* **54** (1986) 375.
29. M. YAMAGUCHI, V. PAIDAR, D. P. POPE and V. VITEK, *ibid.* **45** (1982) 867.
30. V. PAIDAR, M. YAMAGUCHI, D. P. POPE and V. VITEK, *ibid.* **45** (1982) 883.
31. S. M. OHR, *Mater. Sci. Engng* **72** (1985) 1.
32. S. M. OHR and J. NARAYAN, *Phil. Mag.* **41** (1980) 81.
33. S. KOBAYASHI and S. M. OHR, *Scripta Metall.* **15** (1981) 343.
34. *Idem., J. Mater. Sci.* **19** (1984) 2273.
35. S. M. FOILES and M. S. DAW, *J. Mater. Res.* **2** (1987) 5.
36. F. X. KAYSER and C. STASSIS, *Phys. Status Solidi (a)* **64** (1981) 335.
37. S. M. COPLEY and B. H. KEAR, *Trans. AIME* **239** (1967) 977.
38. U. INMAN and H. TIPLER, *Metall. Rev.* **8** (1963) 105.
39. P. S. VENKATESAN and D. N. BESHERS, *J. Appl. Phys.* **41** (1970) 42.
40. J. R. RICE and R. THOMSON, *Phil. Mag.* **29** (1974) 73.
41. P. COULOMB, *J. Microsc. Spectrosc. Electron.* **3** (1978) 295.
42. F. PRINZ, H. O. K. KIRCHNER and G. SCHOECK, *Phil. Mag.* **38** (1978) 321.
43. B. R. LAWN and T. R. WILSHAW, "Fracture of Brittle Solids" (Cambridge University Press, 1975).
44. J. F. KNOTT, "Fundamentals of Fracture Mechanics" (Wiley, New York, 1973).
45. M. H. YOO and A. H. KING, *J. Mater. Res.* **3** (1988) 848.
46. *Idem.*, "Symposium Proceedings on Interface Science and Engineering", ASM World Materials Congress (27–30 September 1988), Chicago, in press.
47. E. SMITH and G. T. BARNBY, *J. Metall. Sci.* **1** (1967) 56.
48. A. BALL and R. E. SMALLMAN, *Acta Metall.* **14** (1966) 1517.
49. M. RUDY and G. SAUTHOFF, *Mater. Sci. Engng* **81** (1986) 525.
50. F. LAVES, *Naturwiss.* **39** (1952) 546.

Received 27 October 1989
and accepted 24 April 1990